Acta Crystallographica Section A
Foundations of Crystallography
ISSN 0108-7673

Received 3 October 2007
Accepted 16 February 2008

Phase stability in ferroelectric bismuth titanate: a first-principles study

Anurag Shrinagar,[a] Ashish Garg,[a]* Rajendra Prasad[b] and Sushil Auluck[b]

[a]Department of Materials and Metallurgical Engineering, Indian Institute of Technology Kanpur, Kanpur 208016, India, and [b]Department of Physics, Indian Institute of Technology Kanpur, Kanpur 208016, India. Correspondence e-mail: ashishg@iitk.ac.in

Experimental data on the structure of ferroelectric oxide bismuth titanate suggest two different kinds of structures, *i.e.* orthorhombic and monoclinic. Density-functional-theory-based (DFT) first-principles calculations have been performed to determine the most stable structure of bismuth titanate among experimentally observed structures. Orthorhombic and monoclinic phases are optimized to zero pressure and lattice parameters were determined as a = 5.4370, b = 5.4260, c = 32.6833 Å and Z = 4 for the structure with space group $B2cb$, and a = 5.4289, b = 5.4077, c = 32.8762 Å, β = 90.08° and Z = 4 for the structure with space group $B1a1$. Static and relaxation calculations show that the monoclinic structure with space group $B1a1$ is the most stable structure.

1. Introduction

Bismuth layered compounds such as $SrBi_2Ta_2O_9$ and $Bi_4Ti_3O_{12}$ belong to the aurivillius family of phases (Aurivillius, 1949; Smolenski *et al.*, 1961; Subbarao, 1962) and are denoted by a general formula $(Bi_2O_2)^{2+}(A_{n-1}B_nO_{3n+1})^{2-}$, where n represents the number of perovskitic $(A_{n-1}B_nO_{3n+1})^{2-}$ layers which are alternately stacked with fluorite-like $(Bi_2O_2)^{2+}$ layers along the c axis of the unit cell.

Bismuth titanate, $Bi_4Ti_3O_{12}$, with n = 3 has attracted a tremendous amount of attention in the past decade, primarily due to its potential for non-volatile memory applications as its thin films showed good ferroelectric properties and, more importantly, lower processing temperatures than its predecessor $SrBi_2Ta_2O_9$ (Paz de Araujo *et al.*, 1995; Park *et al.*, 1999). However, the structure of $Bi_4Ti_3O_{12}$ has been intriguing because experimental studies report either monoclinic or orthorhombic structured phases. First, in 1949, Aurivillius (1949), based on X-ray diffraction results, conceived its structure as orthorhombic with space group $Fmmm$ and lattice parameters a = 5.410, b = 5.448 and c = 32.8 Å. Later, Dorrian *et al.* (1971) showed that, although the X-ray diffraction data supported an orthorhombic structure with space group $B2cb$ and lattice parameters a = 5.448 (2), b = 5.411 (2), c = 32.83 (1) Å, physical properties indicated a monoclinic structure. The authors also observed a small but finite polarization along the c axis which is an unlikely event because, in the $B2cb$ structure, the b-glide has its mirror plane perpendicular to the c axis so projections of all the polarization vectors along the c axis are canceled.

In 1990, Rae *et al.* (1990) conducted a structure refinement of bismuth titanate using electron diffraction data obtained on single-crystal bismuth titanate and reported the structure to be monoclinic with space group $B1a1$ and lattice parameters a = 5.450 (1), b = 5.4059 (6), c = 32.832 (3) Å and β = 90°. In $B1a1$, the absence of a b-glide plane explained the existence of finite remnant polarization along the c axis. Subsequent refinement of neutron diffraction data by Hervoches & Lightfoot (1999) suggests the structure to be orthorhombic with space group $B2cb$ and lattice parameters a = 5.4444 (1), b = 5.4086 (1) and c = 32.8425 (6) Å. Hervoches & Lightfoot (1999) also mentioned that neutron diffraction studies are not as precise as electron diffraction. Hence, the results of Rae *et al.* (1990) may be more accurate. More recent experimental observations have reported the monoclinic structured phase with space group $B1a1$ (Shimakawa *et al.*, 2001; Kim *et al.*, 2003). The above findings show that the experimentally determined structures of bismuth titanate show subtle differences and are dependent upon the history of the sample. These disparities emphasize the need for a theoretical study to further investigate the experimentally observed structures of bismuth titanate.

Previous structural optimization of $Bi_4Ti_3O_{12}$ was performed by Noguchi *et al.* (2005) on an $I4/mmm$ tetragonal structure but the tetragonal phase of $Bi_4Ti_3O_{12}$ is not a room-temperature phase and is stable only above its Curie temperature of 948 K (Hirata & Yokokawa, 1997). To the best of our knowledge, no structural optimization has been performed on the orthorhombic and monoclinic structures of $Bi_4Ti_3O_{12}$. Such a structure optimization will also be important in resolving some of the disagreements observed in the lanthanide-doped bismuth titanate thin films regarding polarization in c-axis-oriented epitaxial thin films (Chon *et al.*, 2002; Garg *et al.*, 2003; Watanabe *et al.*, 2004). One of the reasons that could lead to observed disparities is substrate-induced strain. In this context, a study on structure prediction

Table 1
Results of static calculations and relaxation conducted on experimental structures.

Static calculations were performed on structures *A*, *B* and *C*, whereas relaxation yielded structures *D* and *E*.

Identification	Space group	Total energy (GGA) per 2 f.u. (eV)†	Total energy (LDA) per 2 f.u. (eV)†	Reference
Structure *A*	*B*2*cb*	−266.50	−297.80	Dorrian *et al.* (1971)
Structure *B*	*B*2*cb*	−275.38	−306.64	Hervoches & Lightfoot (1999)
Structure *C*	*B*1*a*1	−276.97	−308.26	Rae *et al.* (1990)
Structure *D*	*B*2*cb*	−277.25	−308.58	Optimized *B* structure
Structure *E*	*B*1*a*1	−277.31	−308.63	Optimized *C* structure

† f.u: formula units.

will further enable us to theoretically investigate the structural changes in this material that occur upon doping and application of external strain, especially in thin-film form.

In this paper, we present a first-principles study using density functional theory (DFT) on the experimentally observed orthorhombic and monoclinic phases of $Bi_4Ti_3O_{12}$. In our study, we have used the crystallographic data of three experimental studies on $Bi_4Ti_3O_{12}$, performed by Dorrian *et al.* (1971), Rae *et al.* (1990) and Hervoches & Lightfoot (1999). We conducted our calculations for total energy on these experimental structures. We have also calculated the optimized structures of orthorhombic and monoclinic phases.

2. Computational details

The calculations for optimization are performed in the framework of first-principles density functional theory (Dreizler & Gross, 1990; Payne *et al.*, 1992). The Vienna *ab initio* simulation package (*VASP*) (Kresse & Hafner, 1993; Kresse & Furthmuller, 1996*a*,*b*) is used for structural optimization in the present study using the projector augmented wave method (PAW) (Kresse & Joubert, 1999). The Kohn–Sham equations (Hohenberg & Kohn, 1964; Kohn & Sham, 1965) are solved using the exchange correlation function of Perdew & Wang (1992) for a generalized gradient approximation (GGA) scheme and Ceperley & Alder (1980) for local density approximation (LDA). A plane-wave energy cut-off of 400 eV is used. We used Monkhorst–Pack (1977) sampling using the $4 \times 4 \times 4$ mesh. A conjugate-gradient (Press *et al.*, 1986) algorithm is used for structural optimization. The tetrahedron method with Blöchl corrections (Blöchl *et al.*, 1994) is used for *k*-integration to determine the total energy. The calculations are performed at 0 K.

Static calculations are performed on the experimental structures keeping their volume, cell shape and ionic positions fixed. In relaxation, first of all, ions are relaxed into their instantaneous ground state keeping the volume and shape of the unit cell fixed. Later, cell shape is relaxed while keeping its volume and positions of ions fixed to get the optimized structure. This optimized structure is relaxed repeatedly through this process until we get the stable ionic positions up to the accuracy of 10^{-4} in fractional coordinates. Symmetry is kept fixed in fractional coordinates to the accuracy of 10^{-5} during the relaxation process to restore the correct charge density and forces. Forces between the ions are relaxed below 0.005 eV $Å^{-1}$. The volume of the unit cell is changed manually by adjusting the cell constant in the input to get the total pressure equal to zero as well as zero pressure along *x*, *y* and *z* axes of the Cartesian coordinate system.

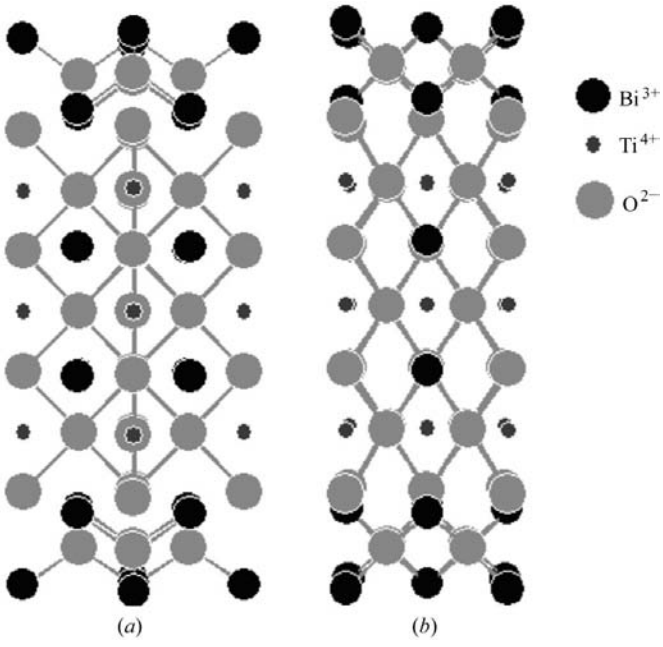

Figure 1
(*a*) A perspective drawing of the *Fmmm* parent phase as viewed along the (110) projection, and (*b*) as viewed along the (100) or (010) projection plane. Only the ions between $c = \frac{1}{4}$ and $c = \frac{3}{4}$ are shown.

3. Results and discussion

The idealized structure of bismuth titanate having space group *Fmmm*, as shown in Fig. 1, was first observed by Aurivillius (1949). The structure consists of $Bi_2O_2^{2+}$ layers alternating with perovskite structured $Bi_2Ti_3O_{10}^{2-}$ layers. However, displacement of *A* cations (Bi^{3+}) along with corresponding cooperative tilting and distortion of TiO_6 octahedra causes deviation from the ideal structure giving rise to the observed ferroelectricity in this compound (Dorrian *et al.*, 1971). Subsequent experimental studies carried out using X-ray, neutron and electron diffraction methods showed that structure of bismuth titanate has space group either *B*2*cb* (Dorrian *et al.*, 1971; Hervoches & Lightfoot, 1999) or *B*1*a*1 (Rae *et al.*, 1990). We began our studies with these three experimental structures as suggested by Dorrian *et al.* (1971) [structure *A* hereafter], Hervoches & Lightfoot (1999) [structure *B* hereafter] and Rae *et al.* (1990) [structure *C* hereafter]. We first calculated the stability of these structures on the basis of energy by conducting static calculations, keeping the

Table 2
Lattice parameters of experimental structures and optimized structures.

Identification	Exchange correlation	a (Å)	b (Å)	c (Å)	β (°)	Space group
Structure A	GGA	5.448 (2)	5.411 (2)	32.83 (1)	–	*B*2*cb* (orthorhombic)
	LDA	5.448 (2)	5.411 (2)	32.83 (1)	–	
Structure *B*	GGA	5.4444 (1)	5.4086 (1)	32.8425 (6)	–	*B*2*cb* (orthorhombic)
	LDA	5.4444 (1)	5.4086 (1)	32.8425 (6)	–	
Structure *C*	GGA	5.450 (1)	5.4059 (6)	32.832 (3)	90	*B*1*a*1 (monoclinic)
	LDA	5.450 (1)	5.4059 (6)	32.832 (3)	90	
Structure *D*	GGA	5.4370	5.4260	32.6833	–	*B*2*cb* (orthorhombic)
	LDA	5.3318	5.3388	32.0061	–	
Structure *E*	GGA	5.4289	5.4077	32.8762	90.08	*B*1*a*1 (monoclinic)
	LDA	5.3151	5.3162	32.2107	90.16	

parameters of all unit cells and their corresponding ionic positions fixed; the results are shown in Table 1.

First we will analyze and compare structures *A* and *B* having the same space group. Table 1 shows that structure *A* exhibits a higher value of energy as compared to structure *B*. We also compared the lattice parameters of these two structures and the values are given in Table 2. It can be seen from the table that cell parameters of the unit cell of structure *A* are nearly the same as the cell parameters of the unit cell of structure *B*. To further analyze this, we compared the ionic positions and the forces on each ion (given in Table 3). The table shows that the forces on each ion in both structures are quite high and hence both these structures are not stable.

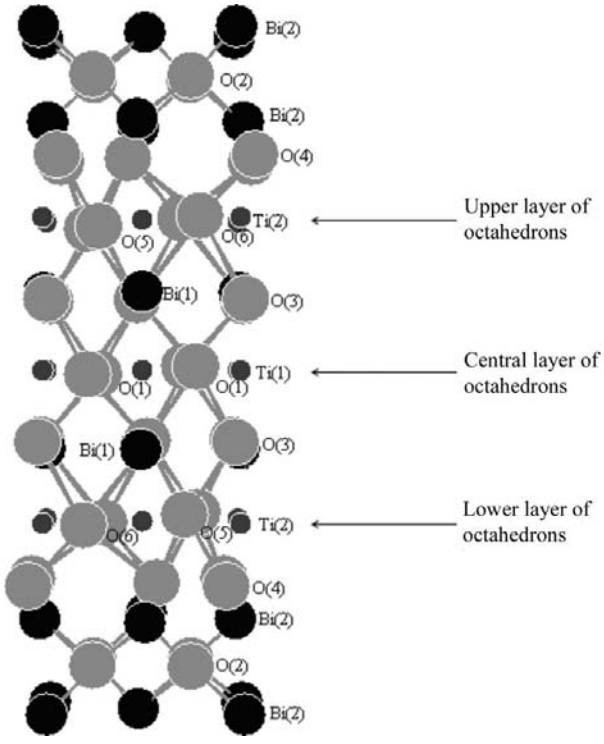

Figure 2
*B*2*cb* structure as observed by Dorrian *et al.* (1971) projected on the (100) plane. Ions are shown between $\frac{1}{4}c$ and $\frac{3}{4}c$ only.

Particularly high values of forces are observed on Ti(1), Ti(2), O(1), O(5) and O(6) ions in structure *A* in comparison to structure *B*. These ions are also depicted in the structure shown in Fig. 2. The figure shows that O(5) and O(6) are the corner ions of the octahedra in the upper and lower layers with Ti(2) located at the center of these octahedra. The O(1) ion is located at the corners of octahedra in the central layer and Ti(1) is located at the center of these octahedra. Comparatively higher values of forces on these ions in structure *A* arise because of significant differences in their positions as compared to structure *B*. These results indicate that the coordinates determined by Hervoches & Lightfoot (1999) for structure *B* are more precise than those determined by Dorrian *et al.* (1971) for structure *A*. The energy differences between structures *A* and *B* is 8.88 eV per 2 formula units (f.u.) for GGA and 8.84 eV for LDA. Thus, as far as energy difference is concerned, LDA and GGA give similar results. Hence our calculations again support the rather precise nature of the ionic positions determined by Hervoches & Lightfoot (1999). On the basis of these observations, we will not consider structure *A* any further and chose structure *B* with space group *B*2*cb* for further optimization along with structure *C* with space group *B*1*a*1.

To reduce the time of calculations, we preferred to conduct our calculations on the primitive unit cells of both the structures. Since both of these structures are *B*-centered and contain two lattice points, their primitive unit cells a', b', c' were chosen. A change in the unit cell also modifies the fractional coordinates from the fraction of *B*-centered unit-cell axes to the fraction of primitive unit-cell axes. Both primitive and parent unit cells follow the condition that the arrangement of ions remains the same in the Cartesian coordinate system as shown in equation (1):

$$x\mathbf{a} + y\mathbf{b} + z\mathbf{c} = x'\mathbf{a}' + y'\mathbf{b}' + z'\mathbf{c}', \qquad (1)$$

where (x, y, z) are the fractional coordinates of an ion with respect to (a, b, c) axes of the *B*-centered non-primitive unit cell and (x', y', z') are fractional coordinates with respect to (a', b', c') axes of the primitive unit cell. The a', b' and c' axes are written in terms of a, b and c in the following manner:

Table 3
Fractional coordinates and total forces (eV Å^{-1}) on the experimental structures under study.

For structure *C* (space group *B*1*a*1), only initial coordinates (x, y, z) are reported but, for structures *A* and *B* (space group *B*2*cb*), equivalent $(x, -y, -z)$ coordinates are also reported.

	Structure *A*				Structure *B*				Structure *C*			
Ion	*x*	*y*	*z*	*F*	*x*	*y*	*z*	*F*	*x*	*y*	*z*	*F*
Bi(1)	0	0.5022 (2)	0.56680 (2)	1.99	0	0.5018 (7)	0.56639 (8)	0.44	0.0030 (1)	0.5023 (1)	0.5673 (1)	0.48
Bi(1)′†	0	−0.5022 (2)	−0.56680 (2)	1.99	0	0.4982 (7)	0.43361 (8)	0.44	0.0013 (1)	0.4977 (1)	0.4336 (1)	0.27
Bi(2)	−0.0009 (3)	0.4801 (1)	0.71135 (2)	0.9	0.001 (1)	0.4861 (9)	0.71127 (8)	0.68	−0.0021 (1)	0.4793 (1)	0.7113 (0)‡	1.07
Bi(2)′	−0.0009 (3)	−0.4801 (1)	−0.71135 (2)	0.9	0.001 (1)	0.5139 (9)	0.28873 (8)	0.68	0.0021 (1)	0.5185 (1)	0.2887 (0)‡	0.25
Ti(1)	0.0452 (8)	0	0.5	4.47	0.052 (2)	0	0.5	0.78	0.0446 (2)	−0.0013 (6)	0.5007 (2)	0.58
Ti(2)	0.0533 (6)	0.0001 (1)	0.6286 (1)	6.61	0.037 (2)	−0.004 (2)	0.6283 (2)	1.41	0.0520 (6)	−0.0004 (4)	0.6289 (2)	0.27
Ti(2)′	0.0533 (6)	−0.0001 (1)	−0.6286 (1)	6.61	0.037 (2)	0.004 (2)	0.3717 (2)	1.41	0.0499 (6)	0.0002 (4)	0.3717 (2)	1.77
O(1)	0.207 (4)	0.278 (5)	0.4967 (8)	3.22	0.322 (2)	0.235 (1)	0.5069 (2)	1.01	0.2990 (12)	0.2760 (12)	0.5102 (3)	0.37
O(1)′	0.207 (4)	−0.278 (5)	−0.4967 (8)	3.22	0.322 (2)	−0.235 (1)	0.4931 (2)	1.01	0.3548 (11)	−0.2179 (11)	0.4942 (3)	0.59
O(2)	0.264 (7)	0.252 (9)	0.2501 (7)	0.91	0.265 (1)	0.263 (1)	0.2485 (2)	0.97	0.2704 (17)	0.2442 (16)	0.2495 (6)	0.97
O(2)′	0.264 (7)	−0.252 (9)	−0.2501 (7)	0.91	0.265 (1)	0.737 (1)	0.7515 (2)	0.97	0.2736 (16)	0.7571 (16)	0.7489 (6)	0.65
O(3)	0.073 (4)	0.025 (6)	0.5596 (8)	1.27	0.086 (1)	−0.0640 (9)	0.5594 (2)	0.65	0.0913 (18)	−0.0705 (16)	0.5605 (4)	0.05
O(3)′	0.073 (4)	−0.025 (6)	−0.5596 (8)	1.27	0.086 (1)	0.0640 (9)	0.4406 (2)	0.65	0.0918 (18)	0.0587 (16)	0.4424 (4)	0.37
O(4)	−0.040 (4)	0.074 (5)	0.6815 (8)	1.63	0.052 (1)	0.0547 (9)	0.6807 (1)	1.43	0.0552 (24)	0.0584 (19)	0.6825 (5)	0.25
O(4)′	−0.040 (4)	−0.074 (5)	−0.6815 (8)	1.63	0.052 (1)	−0.0547 (9)	0.3193 (1)	1.43	0.0568 (24)	−0.0441 (19)	0.3195 (5)	2.19
O(5)	0.294 (4)	0.215 (6)	0.6215 (8)	3.49	0.284 (2)	0.247 (2)	0.6109 (2)	0.9	0.2904 (18)	0.2800 (15)	0.6121 (5)	0.13
O(5)′	0.294 (4)	−0.215 (6)	−0.6215 (8)	3.49	0.284 (2)	−0.247 (2)	0.3891 (2)	0.9	0.2962 (18)	−0.2659 (16)	0.3892 (5)	0.13
O(6)	0.159 (4)	−0.300 (5)	0.6310 (8)	4.74	0.217 (2)	−0.299 (2)	0.6244 (2)	0.67	0.3677 (17)	−0.1959 (15)	0.6244 (4)	0.54
O(6)′	0.159 (4)	0.300 (5)	−0.6310 (8)	4.74	0.217 (2)	0.299 (2)	0.3756 (2)	0.67	0.3496 (17)	0.2164 (15)	0.3773 (4)	0.35

† For *B*2*cb* structure, ()′ coordinates are generated by twofold rotation about the *x* axis. ‡ Zero e.s.d.'s are given in the original publication (Rae *et al.*, 1990).

$$\mathbf{a}' = (\mathbf{a} - \mathbf{c})/2 \quad (2)$$

$$\mathbf{b}' = \mathbf{b} \quad (3)$$

$$\mathbf{c}' = (\mathbf{a} + \mathbf{c})/2. \quad (4)$$

Regardless of the values of **a**, **b** and **c** in the Cartesian coordinate system, the solution of the above three equations is always $x' = x - z$, $y' = y$ and $z' = x + z$. So after calculating these data, our optimization is conducted finally on the primitive unit cell of both of these structures which contains a total of 38 ions. The primitive unit cell of a structure with space group *B*1*a*1 is equivalent to its original Bravais lattice with space group *P*1*n*1 in which the equivalent positions for the space group *B*1*a*1, $(x,\ y, z)$ and *a*: $(x + \frac{1}{2}, -y + \frac{1}{2}, z)$, change to (x, y, z) and *n*: $(x + \frac{1}{2}, -y + \frac{1}{2}, z + \frac{1}{2})$ as shown in Fig. 3.

Although, on the basis of energy, from Table 1, it can be seen that structure *C* (monoclinic) is more stable than structure *B* (orthorhombic), we proceeded with the further optimization of both of the structures for better precision. Relaxation of structures *B* and *C* yields the optimized structures which we have denoted as structures *D* (space group *B*2*cb*) and *E* (space group *B*1*a*1), respectively. Energy and cell parameters of structures *B*, *C*, *D* and *E* are reported in Table 1 and Table 2, respectively. Fractional coordinates of structures *B* and *C* are given in Table 3 and those of structures *D* and *E* in Table 4. For structures *D* and *E*, we have shown only those coordinates which have been calculated by GGA calculations as previous studies (Kohn & Vashishta, 1983; Prasad *et al.*, 2005) showed that GGA calculations yield cell structure results with higher precision. We can see from Table 2 that the lattice parameters calculated by GGA are closer to the experimentally determined parameters compared to LDA. This is not surprising because LDA is known to underestimate the lattice parameters (Kohn & Vashishta, 1983; Prasad *et al.*, 2005). In the final representation of structure *D*, coordinate axes have been rotated by 180° about the *c* axis and the origin is shifted by *a*/2 and *b*/2 along the +*a* axis and the +*b* axis, respectively. This change of coordinate axes changes the (x, y, z) coordinates of all the ions to $(-x + \frac{1}{2}, -y + \frac{1}{2}, z)$.

Table 4
Fractional coordinates of structures *D* and *E*, calculated by GGA.

For structure *E* (space group *B*1*a*1), only initial coordinates (x, y, z) are reported but, for structure *D* (space group *B*2*cb*), equivalent $(x, -y, -z)$ coordinates are also reported.

	Structure *D*			Structure *E*		
Ion	*x*	*y*	*z*	*x*	*y*	*z*
Bi(1)	0†	0.4959	0.5662	0	0.4965	0.5664
Bi(1)′‡	0	0.5041	0.4338	0.0009	0.4975	0.4337
Bi(2)	−0.0002	0.4809	0.7110	−0.0067	0.4812	0.7105
Bi(2)′	−0.0002	0.5191	0.2890	−0.0025	0.5175	0.2884
Ti(1)	0.0338	0‡	0.5‡	0.0353	−0.0028	0.5015
Ti(2)	0.0448	−0.0039	0.6284	0.0446	−0.0037	0.6288
Ti(2)′	0.0448	0.0039	0.3716	0.0426	0	0.3715
O(1)	0.3073	0.2480	0.5107	0.2741	0.2862	0.5115
O(1)′	0.3073	−0.2480	0.4893	0.3531	−0.2049	0.4935
O(2)	0.2622	0.2464	0.2511	0.2585	0.2462	0.2509
O(2)′	0.2622	0.7536	0.7489	0.2582	0.7536	0.7490
O(3)	0.0789	−0.0774	0.5591	0.0792	−0.0768	0.5604
O(3)′	0.0789	0.0774	0.4409	0.0773	0.0679	0.4428
O(4)	0.0435	0.0574	0.6821	0.0454	0.0582	0.6824
O(4)′	0.0435	−0.0574	0.3179	0.0401	−0.0546	0.3181
O(5)	0.2811	0.2801	0.6102	0.2781	0.2842	0.6109
O(5)′	0.2811	−0.2801	0.3898	0.2827	−0.2737	0.3900
O(6)	0.3624	−0.1941	0.6255	0.3644	−0.1922	0.6264
O(6)′	0.3624	0.1941	0.3745	0.3498	0.2041	0.3762

† Coordinates kept fixed for comparison of different structure. ‡ For *B*2*cb* structure, ()′ coordinates are generated by twofold rotation about the *x* axis.

Table 5
Bond lengths (Å) and bond angles (°) in structure *D*.

Bismuth oxide layer	
Bi(2)—O(2)	2.297, 2.399, 2.238
Perovskite layer	
Bi(1)—O(3)	2.366, 3.149, 2.343, 3.187
Central octahedron	
Ti(1)—O(1)	1.873, 2.036
Ti(1)—O(3)	1.991
O(1)—Ti(1)—O(1)	174.2
O(3)—Ti(1)—O(3)	165.8
Upper octahedron and lower octahedron	
Ti(2)—O(5)	1.971, 2.093
Ti(2)—O(6)	1.918, 2.014
Ti(2)—O(4)	1.784
Ti(2)—O(3)	2.309
O(6)—Ti(2)—O(5)	158.8, 157.7
O(3)—Ti(2)—O(4)	175.6

Coordinate axes are changed to obtain the same format of the fractional coordinates in both structures *D* and *E*. It is noticed from Table 1 that after relaxation the energy of structure *D* (space group *B*2*cb*) decreases by 1.87 eV per 2 f.u. (GGA), *i.e.* from structure *B* to structure *D*. This decrease in the energy creates a few subtle changes in structure *D* from its parent

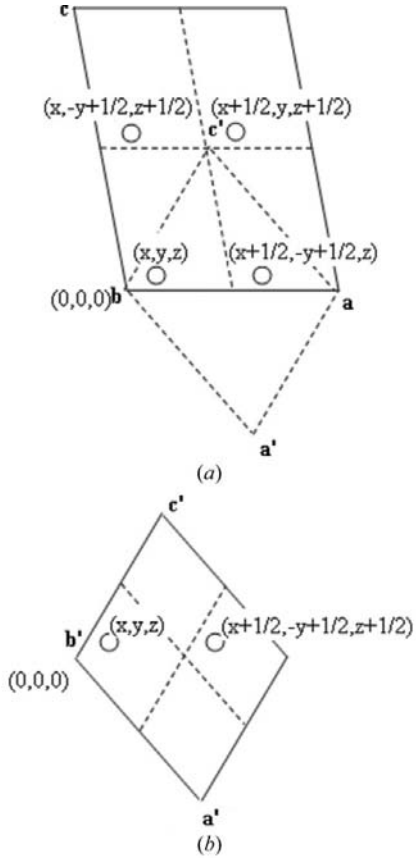

Figure 3
(*a*) Solid lines show *B*-centered unit cell and circles show the general equivalent points generated by the *B*1*a*1 operation. Dashed lines show the simple monoclinic unit cell with a', b' and c' axes. (*b*) General equivalent points of space group *P*1*n*1 in a unit cell with a', b' and c' axes. The *n*-glide is located at $y = \frac{1}{4}$.

Table 6
Bond lengths (Å) and bond angles (°) in structure *E*.

Bismuth oxide layer	
Bi(2)—O(2)	2.238, 2.312
Bi(2)—O(2)′	2.300, 2.416
Bi(2)′—O(2)	2.287, 2.384
Bi(2)′—O(2)′	2.284, 2.234
Perovskite layer	
Bi(1)—O(3)	2.355, 3.136, 2.333, 3.181
Bi(1)′—O(3)′	2.379, 3.127, 2.346, 3.163
Central octahedron	
Ti(1)—O(1)	1.869, 2.057
Ti(1)—O(1)′	1.883, 2.059
Ti(1)—O(3)	1.991
Ti(1)—O(3)′	1.981
O(1)′—Ti(1)—O(1)	172.4
O(3)—Ti(1)—O(3)′	166.5
Upper octahedron	
Ti(2)—O(5)	1.961, 2.093
Ti(2)—O(6)	1.915, 2.015
Ti(2)—O(4)	1.794
Ti(2)—O(3)	2.291
O(6)—Ti(2)—O(5)	158.4, 159.5
O(3)—Ti(2)—O(4)	175.1
Lower octahedron	
Ti(2)′—O(5)′	1.964, 2.063
Ti(2)′—O(6)′	1.919, 2.005
Ti(2)′—O(4)′	1.780
Ti(2)′—O(3)′	2.380
O(5)′—Ti(2)′—O(6)′	156.8, 156.4
O(3)′—Ti(2)′—O(4)′	175.8

structure *B* as seen in Tables 2–4. Table 2 shows that the *c*-axis length of structure *D* decreases by 0.16 Å (GGA) but the rest of the cell parameters of structure *D* do not change appreciably. Comparison of Tables 3 and 4 shows that, in structure *D*, ionic coordinates of the O(6) atom change substantially: the O(6) atom is displaced along the $+a$ axis by 0.79 Å and along the *b* axis by 0.56 Å on both sides of the *c*-glide plane in opposite directions. This change is also shown by arrows in the corresponding structures in Figs. 4(*a*) and 4(*b*), projected on the $(0\bar{1}0)$ plane. The rest of the ions do not show any significant change. In structure *B*, Ti(2) ions are displaced along the $+a$ axis and Ti(1) ions are displaced along the $-a$ axis from the center of their oxygen octahedra. But after optimization, in structure *D*, the observed shift of the O(6) atom along the $+a$ axis makes the Ti(2) ions also displace along the $-a$ axis from the center of their oxygen octahedra and therefore the optimized *B*2*cb* unit cell shows the same polarization direction along the *a* axis as in structures *C* and *E*.

After optimization of structure *C* to structure *E* with space group *B*1*a*1, the energy decreases by 0.44 eV per 2 f.u. (GGA). The relatively smaller change in the energy leads to a very close resemblance between structures *C* and *E* in terms of lattice parameters (Table 2, refer only to GGA) and atomic positions (Table 4). The optimized structure *E* is also represented in Fig. 4(*c*) projected on $(0\bar{1}0)$.

Now we can compare the optimized structure *D* (space group *B*2*cb*) with structure *E* (space group *B*1*a*1). On the basis of lower energy as shown in Table 1, it can be stated that structure *E* is more stable than structure *D*. However, by studying the coordinates of ions in structures *D* and *E* as seen

in Table 4, we observed a close resemblance between the two structures. Major differences are observed only in the coordinates of O(1) and O(1)′ ions: the x and y coordinates of O(1) in structures D and E differ by 0.18 and 0.22 Å and those of O(1)′ differ by 0.25 and 0.25 Å, respectively. For other ions, the differences in coordinates are comparatively very low. These observations suggest that these differences in the ionic positions are because of the presence of a twofold axis and a b-glide plane in the $B2cb$ structure and, when these symmetries are allowed to relax, the coordinates re-adjust themselves to yield a more stable structure E (space group $B1a1$). In the parent structure (space group $Fmmm$), the O and Ti ions located at $x = \frac{1}{4}$ and $x = \frac{1}{2}$ are shifted along the $+a$ axis in both $B2cb$ and $B1a1$ structures (B and C or D and E) (refer also to Fig. 4).

We have also determined the density of states (DOS) and band structures of structures D and E and the results are shown in Figs. 5 and 6, respectively. The density of states and the band structure of both the structures are very similar. On analyzing the partial DOS, we find that O p orbitals dominate at the top of the valence band and Ti d orbitals dominate at the bottom of conduction band. This is in agreement with the work of Postnikov *et al.* (1995). However, we cannot make a precise comparison because Postnikov *et al.* calculated the DOS of the $I4/mmm$ structure of bismuth titanate. Fig. 6 shows that the conduction band minimum lies at Γ and the valence band maximum lies between Γ and S (Y) resulting in an indirect band gap of 2.22 (2.16) eV for the orthorhombic (monoclinic) structure.

Results of calculations on bond lengths and bond angles of structure D and structure E are given in Tables 5 and 6. Bond angles and bond lengths of structures D and E are quite close to each other since the ionic coordinates and cell parameters of both of these structures are very similar as seen in Table 4 and Table 2, respectively. An analysis of the bond lengths and bond angles of both structures shows that there is a significant difference in the two bond lengths of Ti(2)—O(6), Ti(2)′—O(6)′, Ti(2)—O(5), Ti(2)′—O(5)′, Ti(1)—O(1) and Ti(1)—O(1)′. Therefore all the Ti^{4+} ions are shifted along the $-a$ axis from the center of their oxygen octahedra. The displacement of Ti^{4+} ions from the center of their oxygen octahedra for the central layer octahedra is much larger as compared to those in the upper and lower layer octahedra, *e.g.* in structure D (space group $B2cb$), the bond-length difference in two bonds of Ti(1)—O(1) is 0.163 Å while the bond-length differences of Ti(2)—O(5) and Ti(2)—O(6) are 0.122 and 0.096 Å, respectively. Hence, the bond-length difference of Ti(1)—O(1) bonds is more than the bond-length differences of Ti(2)—O(5) and Ti(2)—O(6) bonds, giving rise to a larger shift of the Ti(1) atom along the $-a$ axis than the Ti(2) atom. The same can also be observed in structure E (space group $B1a1$). The shift of Ti along the $-a$ direction is the main reason for higher values of polarization along the a axis as observed in many experimental studies. In structure E, Ti(2)—O(4) and Ti(2)′—O(4)′, Ti(2)—O(3) and Ti(2)′—O(3)′, and Ti(1)—O(3) and Ti(1)—O(3)′ bond lengths in the upper, central and lower octahedra are not equal. But, in structure D, because of the presence of the b-glide plane, these bond lengths are equal. In this structure, the magnitudes of the shifts of the Ti atoms in the upper octahedron and the lower octahedron are the same but in opposite directions along the c axis, and, in the central octahedron, the Ti atom is placed at the center along the c axis, thus causing the polarization along the c axis to be zero in $B2cb$ structure D. On the other hand, in structure E with space group $B1a1$, the bond lengths in the upper, central and lower octahedra are not equal. Therefore, in the $B1a1$ phase, a finite value of polarization is expected along the c axis.

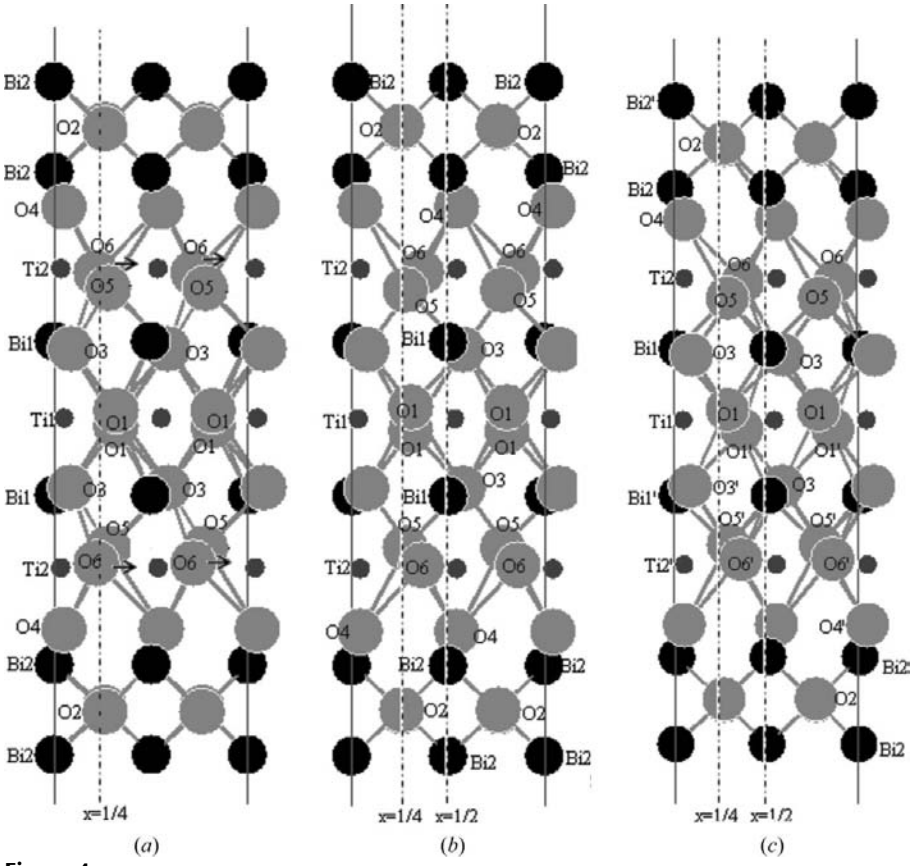

Figure 4
(*a*) Schematic representation of structure B. In this structure, arrows show the displacement of O(6) ions observed after optimization. (*b*) Schematic representation of structure D. (*c*) Schematic representation of structure E. In all the structures, ions are shown only between $\frac{1}{4}c$ and $\frac{3}{4}c$ and projection of unit cells is taken on the $(0\bar{1}0)$ plane. For the $B2cb$ structure, ()′ are shown by () only, since they are equivalent $(x, -y, -z)$ points.

In the end, however, comparison of energies of structure *D* and structure *E* suggests that the lowest-energy structure is the monoclinic structure (structure *E*). However, the differences between the structures are very subtle. The situation may further be complicated by the volatility of bismuth leading to bismuth nonstoichiometry and any oxygen nonstoichiometry which may change the energetics and the ultimate stability of the structure.

4. Conclusions

We have performed an analysis on the structural stability of ferroelectric oxide bismuth titanate by first-principles density functional calculations using experimental data (Dorrian *et al.*, 1971; Rae *et al.*, 1990; Hervoches & Lightfoot, 1999). First the precision of the structures from different experimental studies was compared and analyzed *via* static calculations made on the basis of energy. The results suggest that the structure with space group *B*2*cb* (*B*) predicted by Hervoches & Lightfoot (1999) was more precise than the similar structure (*A*), shown previously by Dorrian *et al.* (1971), the latter exhibiting higher values of forces on its ions and higher total energy. However, the structure with space group *B*1*a*1 (*C*) predicted by Rae *et al.* (1990) appeared to be more precise than structure *B* with space group *B*2*cb*. Further, relaxation was carried out on structures *B* and *C* to yield the optimized structures *D* and *E*, respectively. We found the structure with space group *B*1*a*1 (*E*) to be the most stable structure with minimum energy. However, it must be noted that, although structure *E* with space group *B*1*a*1 has lower energy than structure *D* with space group *B*2*cb*, the energy difference between these two structures is very small, also confirmed by the close resemblance between the unit-cell parameters and fractional coordinates of the structures. A study of the bond lengths and bond angles of *B*1*a*1 structure *E* reveals that, because of the absence of a *b*-glide, polarization along the *c* axis would also be observed in this structure, which is found to be zero in the *B*2*cb* structure *D*. We observed that all Ti ions are shifted towards the $-a$ axis in each octahedron, indicating the presence of a finite polarization along the *a* axis. The DOS and band structure of structures *D* and *E* are very similar and thus

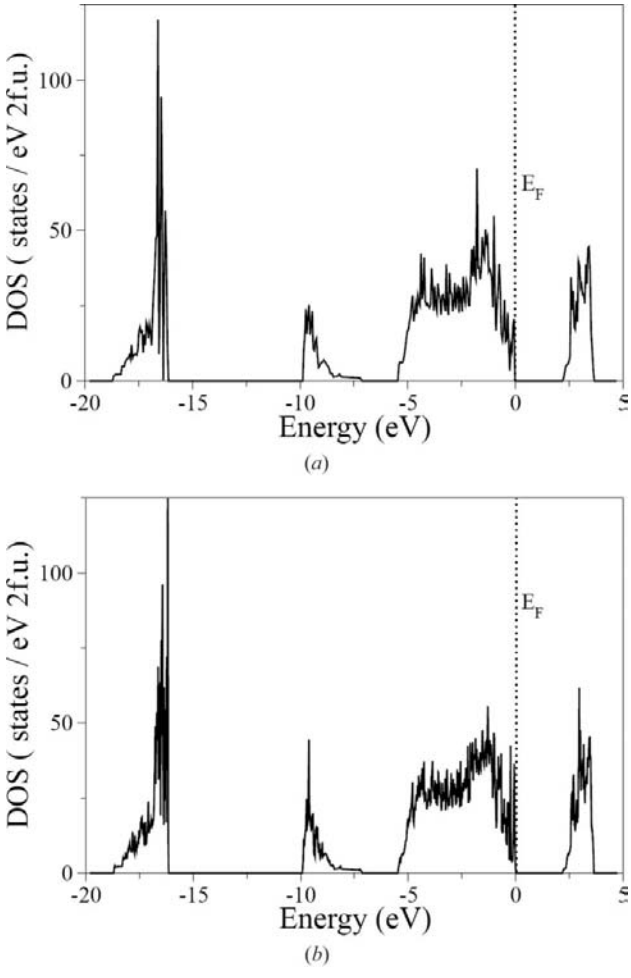

Figure 5
Total density of states (solid lines) is shown for (*a*) structure *D* and (*b*) structure *E*. Fermi energy is referred to the origin of the *x* axis.

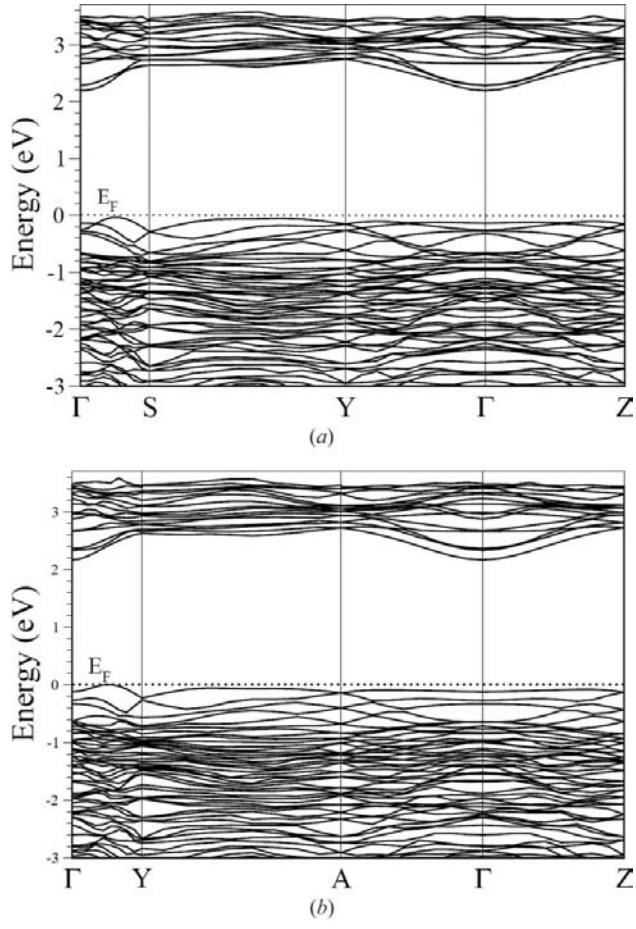

Figure 6
Band structure, along symmetry lines, near the Fermi energy (zero of energy axis) for (*a*) structure *D*, (*b*) structure *E*. The indirect energy gaps are 2.22 and 2.16 eV, respectively. *S* and *Y* points for face-centered orthorhombic correspond to *Y* and *A*, respectively, in simple monoclinic.

it is hard to predict any differences between the two structures on the basis of DOS and band structure.

We thank Dr Arjit Sen and Dr Shailesh Shukla, who have been very helpful in carrying out this whole research.

References

Aurivillius, B. (1949). *Ark. Kemi*, **1**, 499–512.
Blöchl, P. E., Jepsen, O. & Andersen, O. K. (1994). *Phys. Rev. B*, **49**, 16223.
Ceperley, D. M. & Alder, B. J. (1980). *Phys. Rev. Lett.* **45**, 566–569.
Chon, U., Jang, H. M., Kim, M. G. & Chang, C. H. (2002). *Phys. Rev. Lett.* **89**, 087601.
Dorrian, J. F., Newnham, R. E. & Smith, D. K. (1971). *Ferroelectrics*, **3**, 17–27.
Dreizler, R. M. & Gross, E. K. U. (1990). *Density Functional Theory.* Berlin: Springer-Verlag.
Garg, A., Barber, Z. H., Dawber, M., Scott, J. F., Snedden, A. & Lightfoot, P. (2003). *Appl. Phys. Lett.* **83**, 2414–2416.
Hervoches, C. H. & Lightfoot, P. (1999). *Chem. Mater.* **11**, 3359–3364.
Hirata, T. & Yokokawa, T. (1997). *Solid State Commun.* **104**, 673–677.
Hohenberg, P. & Kohn, W. (1964). *Phys. Rev.* **136**, B864–B871.
Kim, Y. I., Jeon, M. K. & Woo, S. I. (2003). *J. Mater. Sci. Lett.* **22**, 1655–1657.
Kohn, W. & Sham, L. J. (1965). *Phys. Rev.* **140**, A1133–A1138.
Kohn, W. & Vashishta, P. (1983). *General Density Functional Theory: Inhomogeneous Electron Gas*, edited by N. H. March & S. Lundqvist, pp. 79–184. New York: Plenum Press.
Kresse, G. & Furthmuller, J. (1996*a*). *Comput. Mater. Sci.* **6**, 15–50.
Kresse, G. & Furthmuller, F. (1996*b*). *Phys. Rev. B*, **54**, 11169–11186.
Kresse, G. & Hafner, J. (1993). *Phys. Rev. B*, **48**, 13115–13118.
Kresse, G. & Joubert, J. (1999). *Phys. Rev. B*, **59**, 1758–1775.
Monkhorst, H. J. & Pack, J. D. (1977). *Phys. Rev. B*, **13**, 5188–5192.
Noguchi, Y., Sogai, M., Takahashi, M. & Miyayama, M. (2005). *Jpn. J. Appl. Phys.* **44**, 6998–7002.
Park, B. H., Kang, B. S., Bu, S. D., Noh, T. W., Lee, J. & Jo, W. (1999). *Nature (London)*, **401**, 682–684.
Payne, M. C., Teter, M. P., Allan, D. C., Arias, T. A. & Joannopoulos, J. D. (1992). *Rev. Mod. Phys.* **64**, 1045–1097.
Paz de Araujo, C. A., Cuchlaro, J. D., McMillan, L. D., Scott, M. C. & Scott, J. F. (1995). *Nature (London)*, **374**, 627–629.
Perdew, J. P. & Wang, Y. (1992). *Phys. Rev. B*, **45**, 13244–13249.
Postnikov, A. V., Bartkowski, St., Mersch, F., Neumann, M., Kurmaev, E. Z., Cherkashenko, V. M., Nemnonov, S. N. & Galakhov, V. R. (1995). *Phys. Rev. B*, **52**, 16–19.
Prasad, R., Benedek, R. & Thackeray, M. M. (2005). *Phys Rev. B*, **71**, 134111.
Press, W. H., Flannery, B. P., Teukolsky, S. A. & Vetterling, W. T. (1986). *Numerical Recipes.* Cambridge University Press.
Rae, A. D., Thompson, J. G., Withers, R. L. & Willis, A. C. (1990). *Acta Cryst.* B**46**, 474–487.
Shimakawa, Y., Kubo, Y., Tauchi, Y., Asano, S., Kamiyama, T., Izumi, F. & Hiroi, Z. (2001). *Appl. Phys. Lett.* **79**, 2791–2793.
Smolenski, G. A., Isupov, V. A. & Agranovskaya, A. I. (1961). *Sov. Phys. Solid State*, **3**, 651–655.
Subbarao, E. C. (1962). *J. Phys. Chem. Solids*, **23**, 665–676.
Watanabe, T., Kojima, T., Uchida, H., Okada, I. & Funakubo, H. (2004). *Jpn. J. Appl. Phys.* **43**(2B), L309–L311.